RESEARCH ARTICLE
SOLID EARTH: PALEOMAGNETISM

Earth and Planetary Physics
6: 359–365, 2022
doi: 10.26464/epp2022030

A new inclination-based method to evaluate the global geomagnetic configuration and axial dipole moment

KaiHua Xu[1,2,3], Fei He[1,2*], Yong Wei[1,2], Ross N. Mitchell[1,2], Si Chen[1,2], YuQi Wang[1,2], and ZhaoJin Rong[1,2]

[1]Key Laboratory of Earth and Planetary Physics, Institute of Geology and Geophysics, Chinese Academy of Sciences, Beijing 100029, China;

[2]College of Earth and Planetary Sciences, University of Chinese Academy of Sciences, Beijing 100049, China;

[3]School of Earth and Environment, University of Leeds, Leeds, LS2 9JT, UK

Key Points:

- Globally distributed inclination records were used to characterize the magnetic field configuration.
- The axial dipole moment can be estimated from the magnetic field configuration and the virtual dipole moment by using an empirical formula.
- The estimated axial dipole moment is underestimated by approximately three times the virtual dipole moment during the Laschamp excursion, consistent with the results of paleomagnetic models.

Citation: Xu, K. H., He, F., Wei, Y., Mitchell, R. N., Chen, S., Wang, Y. Q., and Rong, Z. J. (2022). A new inclination-based method to evaluate the global geomagnetic configuration and axial dipole moment. *Earth Planet. Phys.*, *6*(4), 359–365. http://doi.org/10.26464/epp2022030

Abstract: The strength and configuration of the geomagnetic field control the average shape of the magnetosphere. The pure dipole assumption and the virtual dipole moment (VDM), determined by individual records, have been widely adopted to evaluate the strength of the geomagnetic field in geological time. However, such an assumption might not be valid during geomagnetic transitions, such as reversals and excursions. The traditional spherical harmonic modeling of the geomagnetic field could be difficult to implement because accurate global records are lacking. Here, we report that an empirical relationship exists between the ratio of the VDM to the true axial dipole moment (VDM/ADM) and the ratio of the power of the axial dipole to that of the non-axial dipole (AD/NAD) based on a new method utilizing globally distributed inclination records. The root mean square global deviation of inclination (RMSΔI) to the standard inclination distribution of the AD was fitted to the AD/NAD with a cubic polynomial by utilizing a large number of geodynamo simulations. Tests with geomagnetic field models showed that the AD/NAD derived from the RMSΔI agreed well with that calculated by using the Gauss coefficients, and the estimated ADM was consistent with the true value. Finally, the application of volcanic records during the Laschamp excursion showed the VDM might overestimate the ADM by a factor of 3. Our new method will be useful in future studies that characterize the configuration of the geomagnetic field and the strength of the axial dipole.

Keywords: axial dipole; magnetic inclination; virtual dipole moment

1. Introduction

Characterizing the configuration and evolution of the magnetic field of Earth is central to the investigation of the habitability of the planet over geological time. The geomagnetic field not only blocks the entry of interstellar energetic particles that could damage the Earth's biosphere but also shapes the magnetosphere, which is an extension of the dipole field into space that slows the rate of atmospheric escape into interplanetary space (Wei Y et al., 2014; Tsareva et al., 2020). During a geomagnetic transition time, when the strength of the axial dipole (AD) decreases significantly, the interaction between the solar wind and the magnetosphere changes (Gao JW et al., 2022; Gong F et al., 2022), and the size of the magnetosphere shrinks, allowing energetic particles to reach the low latitudes of Earth (Vogt et al., 2007; Grießmeier et al., 2009; Stadelmann et al., 2010). Therefore, an adequate estimation of the configuration of the paleomagnetic field and the strength of the AD form the foundation for investigating the paleomagnetosphere.

Conventionally, under the geocentric dipole assumption, the virtual dipole moment (VDM; Smith, 1967) derived from magnetic intensity records is applied to assess the strength of the geomagnetic field. A common expression of the VDM (Merrill et al., 1998) is

$$\mathrm{VDM} = \frac{4\pi R_E^3 F}{\mu_0\sqrt{1+3\cos^2\theta}}, \tag{1}$$

where R_E is the radius of the Earth, and F is the intensity (in tesla) of the magnetic field observed at magnetic colatitude θ. The VDM does not represent the true dipole moment but is overestimated (Korte and Constable, 2005). When the geomagnetic field is AD dominant, the VDM can be an adequate approximation of the AD moment (ADM). However, the AD becomes weak during geomag-

Correspondence to: F. He, hefei@mail.iggcas.ac.cn
Received 11 MAR 2022; Accepted 28 MAY 2022.
Accepted article online 28 JUN 2022.

netic transitions (e.g., the Laschamp excursion). The non-dipole component is as critical as the AD (Leonhardt et al., 2009; Korte et al., 2019; Panovska et al., 2019). In this case, both the AD and the non-axial dipole (NAD) make comparable contributions to the VDM, which is no longer a good representation of the ADM. A more appropriate way to distinguish the contribution of the AD and NAD is through a spherical harmonic analysis. The Gauss coefficients can estimate the amplitudes of the AD and other components. Nevertheless, calculating the Gauss coefficients by fitting magnetic records is an inverse problem that affects the modeling strategy, especially when the data are sparsely distributed.

Here, we introduce a new method to estimate the ADM from the VDM without using the Gauss coefficients. Statistical analysis of numerous dynamo simulations demonstrated that the ratio of the VDM to ADM correlates well with the field morphology criterion, AD/NAD (Christensen et al., 2010). The criterion AD/NAD, which reflects the AD dominance of the magnetic field and characterizes morphology, can be computed for the Earth's surface with Gauss coefficients (g_{nm} and h_{nm}) by using the following formula:

$$\mathrm{AD/NAD} = \frac{P_{10}}{P_{11} + \sum_{n=2}^{n_{\max}} \sum_{m=0}^{n} P_{nm}}, \tag{2}$$

$$P_{nm} = (n+1)(g_{nm}^2 + h_{nm}^2). \tag{3}$$

In a recent study, Biggin et al. (2020) reported a new approach for estimating the AD/NAD of the time-averaged field by using the virtual geomagnetic pole dispersion without Gauss coefficients. In this study, we explored dynamo simulations and documented an empirical formula to evaluate the AD/NAD from the global distribution of inclination (I) data. Numerical simulations of the geodynamo successfully reproduced both the dramatic magnetic reversal (Glatzmaier and Roberts, 1995) and the common features of the paleomagnetic field (Davies and Constable, 2014; Meduri et al., 2021). In this manner, we can simulate both the transitional field and the stable field, which means that the magnetic field morphology can range from dipole dominance to multipole dominance. Thus, these simulated fields provide a good opportunity to investigate the rule of inclination distribution with wide AD/NAD coverage. Finally, two empirical relationships were established to estimate the AD/NAD from I and the VDM/ADM from the AD/NAD. These relationships became a new tool for estimating the ADM and AD/NAD from paleomagnetic records without using Gauss coefficients.

In Section 2, we introduce the variable substitution of the AD/NAD and the measurement of the inclination distribution, which will help in constructing empirical relationships. Errors from sampling the magnetic records are also analyzed in this section. Empirical relationships are then presented and discussed in Section 3. Finally, in Section 4, we show how these relationships were tested by using various spherical harmonic models and applied to volcanic records from the last 50 ka.

2. Methods

2.1 Variable Substitution of the AD/NAD

The AD/NAD is the criterion that indicates the morphology of a magnetic field; nonetheless, the AD/NAD ratio may vary over a large range. To normalize the range from 0 to 1, we suggest using AD/(AD + NAD) instead of AD/NAD to indicate the dominance of AD. The AD/(AD + NAD) = 1 when the magnetic field is a pure AD. In the following, AD/(AD + NAD) was used to build the empirical formula instead of AD/NAD.

2.2 Measurement of the Inclination Distribution

In an ideal AD field, the inclination I is determined by the colatitude θ as

$$\tan I = 2\cot\theta. \tag{4}$$

It is difficult to determine such an analytical expression of I when the magnetic field is not an AD. To describe the distribution of inclinations observed from an NAD field, we compared the observed inclination value with those predicted by the AD and measured the difference with the root mean square value:

$$\mathrm{RMS}\Delta I = \sqrt{\frac{\sum_{j=1}^{n} \left(I_j^{rec} - I_j^{mod}\right)^2}{n}}, \tag{5}$$

where I_j^{mod} is the inclination value predicted by the AD by using Equation (4) at the same latitude as I_j^{rec}, and n is the number of observed I_j^{rec}. The RMSΔI reflects the degree of deviation of the inclination distribution in the magnetic field relative to the AD field. For example, Figure 1 illustrates the inclination–colatitude distribution (blue circles) calculated with the IMMAB4 model (Leonhardt and Fabian, 2007) at the dipole-dominant time (the end of the reversal at 765 ka; Figure 1a) and the transition time (midpoint of the reversal at 774 ka; Figure 1b). At the dipole-dominant time, the inclination distribution is close to that of AD (black curve), and the RMSΔI value is small (approximately 6). In contrast, at the transition time, they are different and the RMSΔI value can be greater than 60. For a pure AD, the RMSΔI should be 0, by definition. Here, we systematically investigate the relationship between the RMSΔI and field morphology.

The most appropriate way to construct a database of geomagnetic fields with various morphologies is through numerical dynamo simulations that solve the magnetohydrodynamic equations describing the generation of the geomagnetic field from the movement of the conductive fluid in the outer core of the Earth. The geomagnetic fields generated from the dynamo simulations are described well by the spherical harmonic method, and all Gauss coefficients are known, which is appropriate for this study. The dynamo simulations used in this study were similar to those used in previous studies (Davies and Constable, 2014; Sprain et al., 2019; Biggin et al., 2020). Briefly, a rigid spherical shell that contains an incompressible and electrically conducting Boussinesq fluid rotates in the vertical direction with an angular frequency Ω. The width of the shell is $d = r_o - r_i$, where r_o and r_i denote the outer and inner boundary radii, respectively. The simulations numerically solve the equations of evolution for the fluid velocity (u), magnetic field (B), and temperature (T) with the nondimensionalization of the physical parameters in the equations. For nondimensionalization, the magnetic field is rescaled by $(2\Omega\rho\mu_0\eta)^{1/2}$, the length is rescaled by d, the time is rescaled by the magnetic diffusion time,

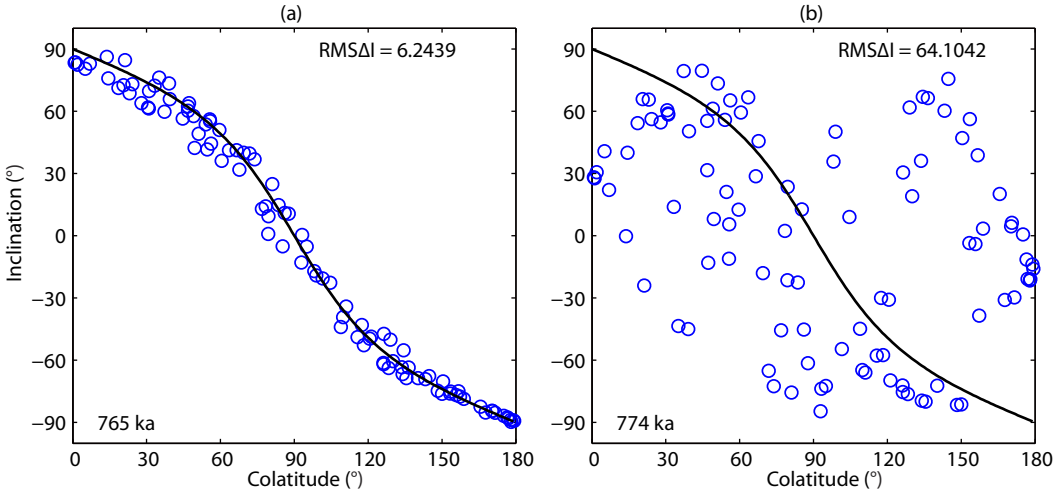

Figure 1. Inclination–colatitude distribution of the IMMAB4 model during (a) the dipole-dominant time and (b) the transition time. The blue circles indicate data obtained from the model. The black line is the inclination–colatitude relationship according to the axial dipole. RMSΔI, root mean square global deviation of inclination.

$\tau_\eta = d^2/\eta$, where η denotes the magnetic diffusivity of the outer core, ρ is the core fluid density, and μ_0 is the vacuum permeability. In this work, the shell aspect ratio r_i/r_o is set to 0.35. In the dynamo simulations, geomagnetic fields of various morphologies were generated with the AD/(AD + NAD) varying from 3.59×10^{-9} to 0.95. This broad coverage of the AD/(AD + NAD) ensured that the empirical relationship would be widely valid.

We also explored the relationship between AD/(AD + NAD) and VDM/ADM based on the dynamo simulations. The main process of the study can be described by the following steps:

(1) For a given geomagnetic field from the dynamo simulations, several locations around the world were randomly chosen to calculate the magnetic inclination and intensity by using Gauss coefficients.

(2) The VDM was calculated from the magnetic inclination and intensity with the combination of Equations (1) and (4) at each location, and their mean value as the VDM was retained in this geomagnetic field.

(3) The inclination data were used to calculate the RMSΔI by using Equations (4) and (5). The ADM was calculated directly from the Gauss coefficient, and AD/(AD + NAD) was evaluated by using Equations (2) and (3).

(4) The above-mentioned steps were repeated in all dynamo simulation fields to investigate the empirical relationships between RMSΔI and AD/(AD + NAD) and between AD/(AD + NAD) and VDM/ADM. In the following section, we discuss the error from the random selection of data points.

2.3 Error from Record Quantity

One realistic scenario is that finite discrete magnetic records around the world could be collected to evaluate the RMSΔI and VDM. Therefore, a concern is acquiring the appropriate number of records to obtain a reliable RMSΔI and VDM. Here, a record refers to a vector observation or record of the geomagnetic field (including the intensity, inclination, and declination) at an arbitrary location point on the surface of the Earth. Consequently, we calculated the RMSΔI with record number n varying from 1 to 100 with an interval of 1. Specifically, at each time, we randomly chose n locations on the surface of the Earth to calculate the magnetic inclination from the Gauss coefficients and evaluate the RMSΔI. This process was repeated 20 times to obtain the mean value and standard deviation of the RMSΔI for the same n value. Figures 2a–2c illustrate the variations in the mean value, standard deviation (SD), and standard error (SE) of the RMSΔI with n value, respectively, and two geomagnetic field morphologies for dipole dominated (AD/(AD + NAD) = 0.79; in blue) and for multipole dominated (AD/(AD + NAD) = 0.08; in red). As shown in Figure 2, both the mean RMSΔI and its fluctuation amplitude (i.e., the SD and SE) converged with an increase in the number of records for both field morphologies. Figure 2d depicts the variations in the relative SE (RSE) of the RMSΔI (the ratio of the SE to the mean RMSΔI) with the number of records and AD/(AD + NAD). The relative SE of RMSΔI was found to be less than 5% when n exceeded 25 and less than 1% when n was larger than 100 for all morphologies, indicating that a large sample size was not needed to obtain accurate results.

3. Results

3.1 Empirical Relationship Between AD/(AD + NAD) and the RMSΔI

Here, n = 1,500 records were used to calculate the RMSΔI, and the corresponding SD and RSE were less than 1% and 0.1%, respectively. The AD/(AD + NAD) values of the geomagnetic fields from the dynamo simulations varied from 3.59×10^{-9} to 0.95, and the corresponding values of the RMSΔI varied from 80.90 to 7.38. The AD/(AD + NAD) and RMSΔI cross-plot exhibited a significant inverse correlation (Figure 3a). The data were least-squares fitted to the following cubic polynomial (Figure 3a):

$$\mathrm{AD/(AD + NAD)} = p_1\mathrm{RMS\Delta I}^3 + p_2\mathrm{RMS\Delta I}^2 + p_3\mathrm{RMS\Delta I} + p_4, \quad (6)$$

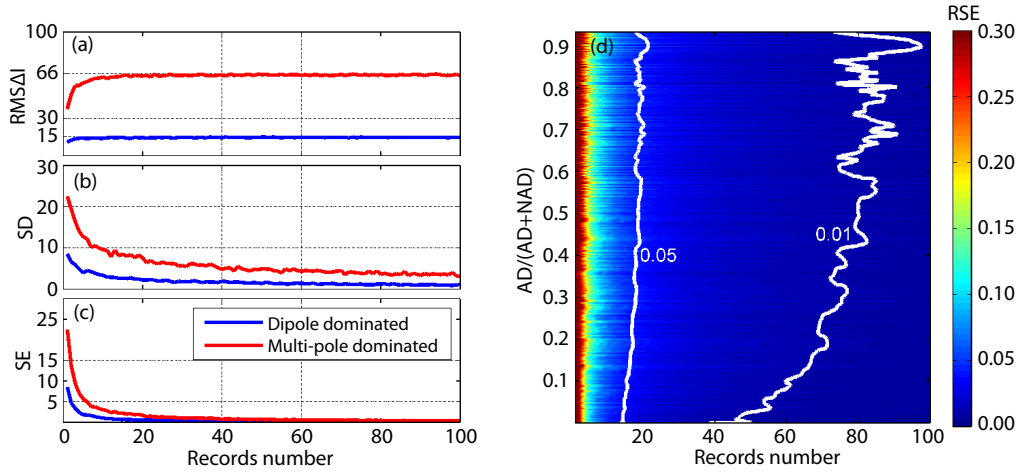

Figure 2. Variations in the (a) root mean square global deviation of inclination (RMSΔI), (b) standard deviation (SD), and (c) standard error (SE) of the RMSΔI versus the record number. The blue curves indicate dipole dominance (AD/(AD + NAD) = 0.79), whereas the red curves indicate nondipole dominance (AD/(AD + NAD) = 0.08). (d) Contour plot of the relative SE (RSE) of the RMSΔI versus record number and field morphology criterion AD/(AD + NAD).

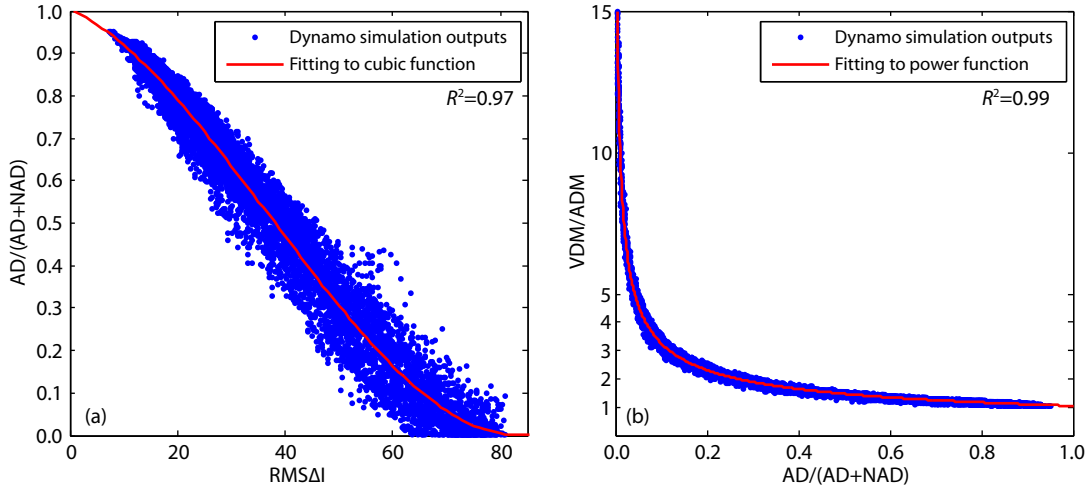

Figure 3. (a) Relationship between the root mean square global deviation of inclination (RMSΔI) and AD/(AD + NAD). The red curve represents the best fit to the cubic function in Equation (6). (b) Relationship between the axial dipole/non-axial dipole (AD/NAD) and virtual dipole moment/axial dipole moment (VDM/ADM). The red curve represents the best fit to the power function in Equation (7). The adjusted r^2 values are indicated in the upper right corners.

where p_1, p_2, p_3, and p_4 equaled 2.67×10^{-6}, -2.978×10^{-4}, -5.757×10^{-3}, and 1.004, respectively. The 95% confidence limits for these four parameters were (2.506×10^{-6}, 2.835×10^{-6}), (-3.192×10^{-4}, -2.764×10^{-4}), (-6.594×10^{-3}, -4.920×10^{-3}), and (0.9944, 1.014), respectively. The adjusted r^2 value of the fit was 0.97, indicating an ideal inverse correlation between AD/(AD + NAD) and the RMSΔI. Empirical Equation (6) predicted that AD/(AD + NAD) would equal 1.004 when the RMSΔI reduced to 0, and this prediction was close to the theoretical value of 1. It should be noted that a zero RMSΔI value indicates that a pure AD geomagnetic field and AD/(AD + NAD) should equal 1.

3.2 Empirical Relationship Between AD/(AD + NAD) and VDM/ADM

We used the same magnetic records from the preceding section to study the empirical relationship between AD/(AD + NAD) and VDM/ADM. As shown in Figure 3b, the VDM/ADM of the geomagnetic field exhibited a significant power law for AD/(AD + NAD). This empirical relationship could be expressed by using the following power equation:

$$\mathrm{VDM/ADM} = a[\mathrm{AD/(AD + NAD)}]^b, \tag{7}$$

where a and b were fitted to 1.045 and −0.4943, respectively, with an adjusted r^2 up to 0.99. The 95% confidence bounds of a and b were (1.042, 1.049) and (−0.4949, −0.4938), respectively. This empirical relationship showed that the VDM would be higher than the ADM when the AD/(AD + NAD) is less than 0.1, whereas the VDM was close to the ADM even though the power of the AD component accounted only for 50% of the total power of the geomagnetic field (i.e., AD/(AD + NAD) = 0.5).

4. Testing the Empirical Formulae and Their Applicability to the Volcanic Records

4.1 Tests with Magnetic Models

Here, the two empirical equations mentioned above were further tested by using different geomagnetic models to verify their performance and applicability. To test geomagnetic fields with various morphologies, models covering both stable and transition times were chosen, including IMMAB4 (Leonhardt and Fabian, 2007), LSMOD.2 (Korte et al., 2019), GGF100k (Panovska et al., 2018), TK03.GAD (Tauxe and Kent, 2004), and the International Geomagnetic Reference Field (IGRF13; Alken et al., 2021). The IMMAB4 simulates the latest geomagnetic reversal at approximately 780 ka, and the LSMOD.2 mainly models the Laschamp excursion at approximately 40 ka. The TK03.GAD is a Giant Gauss Process type statistical model of the geomagnetic field based on paleomagnetic data. The GGF100k is a paleomagnetic model for the past 100 ka, and the IGRF13 mainly covers the recent dipole-dominant period. Thus, these five models included most geomagnetic field situations.

For each geomagnetic model, the RMSΔI and mean VDM were calculated from the inclination and intensity at 100 randomly chosen locations on the surface of the Earth. The AD/(AD + NAD) and ADM values were then calculated by using Equations (6) and (7) and compared with the values derived from the Gauss coefficients. The results of these calculations are shown in Figure 4. The blue dashed diagonal line represents $y = x$, and symbols with different shapes represent different models. In Figure 4a, the estimated AD/(AD + NAD), represented by the gray symbols, is normally distributed around the diagonal. The linear regression (black line) of the symbols is 1.015, with an adjusted r^2 value of 0.96, further demonstrating that the RMSΔI applies to geomagnetic field models with different morphologies. Figure 4b demonstrates that the ADM estimated using Equation (7) (gray points) is very close to the true ADM, and the gray symbols are located near the $y = x$ line. These gray points can be fitted by a black line with an adjusted r^2 value of 0.99. However, the mean VDM values (the calculation is similar to step (2) in Section 2.2, although using the models mentioned in this section), which are denoted by red symbols that scatter away from the $y = x$ line, especially for the IMMAB4 model, indicate that the VDM cannot be an adequate approximation of ADM during times of magnetic reversal. The above-mentioned comparisons with the five geomagnetic field models showed that the two empirical formulae in Section 3 were effective and could play an important role in accurately estimating the ADM from the VDM, particularly during the geomagnetic transition time.

4.2 Implications for the Paleomagnetic Field

Here, we apply the two empirical formulae to the volcanic records of the GEOMAGIA50.v3 data sets (Brown et al., 2015) to investigate the evolution of the magnetic field of the Earth over the past 50 ka. The GEOMAGIA50.v3 is an open database that includes published archaeomagnetic, volcanic, sedimentary, and chronological data (https://geomagia.gfz-potsdam.de/). Considering that the dating errors of the volcanic records vary from several hundred years to several millennia, the following calculation was performed on a 5 ka time average. In every 5 ka time interval, inclination records with α_{95} (95% angular confidence limit around the mean direction) less than 5° were selected and temporally averaged at their locations. Figure 5a shows that the AD/(AD + NAD) curve (in blue) evaluated from the volcanic records dropped dramatically at approximately 25.5–30.5 and 40.5 ka before present (BP), which relates to the Mono Lake (Cassidy and Hill, 2009) and the Laschamp excursion (Guillou et al., 2004), respectively. The AD/(AD + NAD) derived from three paleomagnetic models, GGF100k,

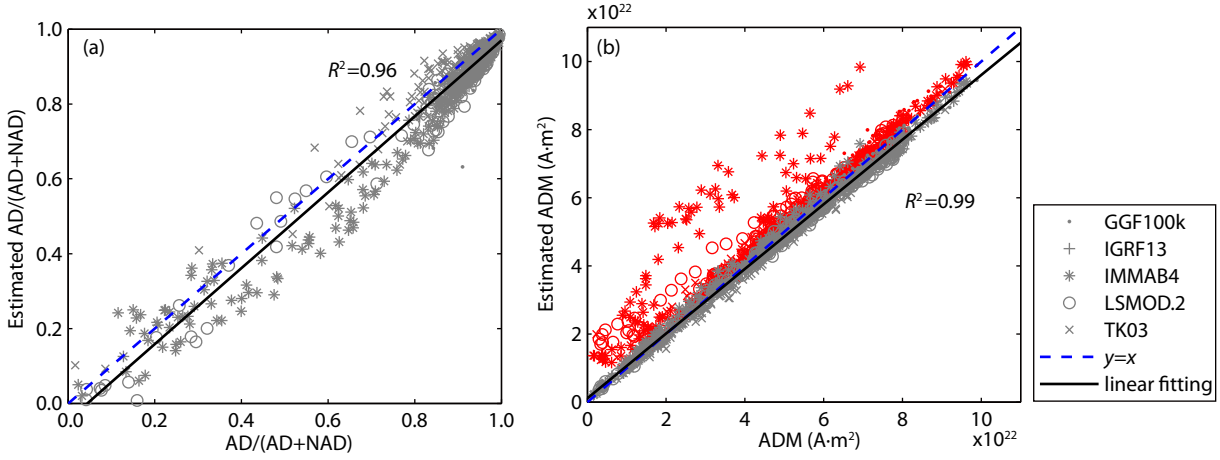

Figure 4. Test of the empirical relationship between (a) the root mean square global deviation of inclination (RMSΔI) and AD/(AD + NAD) and (b) the AD/(AD + NAD) and virtual dipole moment/axial dipole moment (VDM/ADM) with different models. The *x* axis represents the true AD/(AD + NAD) in (a) and ADM in (b) from Gauss coefficients, whereas the *y* axis represents the estimated values with the empirical equations from the corresponding magnetic field. In both panels, the gray points with different shapes are values predicted by the empirical formulae versus the values derived from Gauss coefficients. The different shapes represent different models. The red points in (b) denote the mean VDM versus the true ADM, the blue line is $y = x$, and the black line is a linear regression for all models. The different models are denoted in the legend. The temporal resolutions used for GGF100k, IGRF13, IMMAB4, and LSMOD.02 were 500, 5, 100, and 1,000 years, respectively, for the data points in both panels.

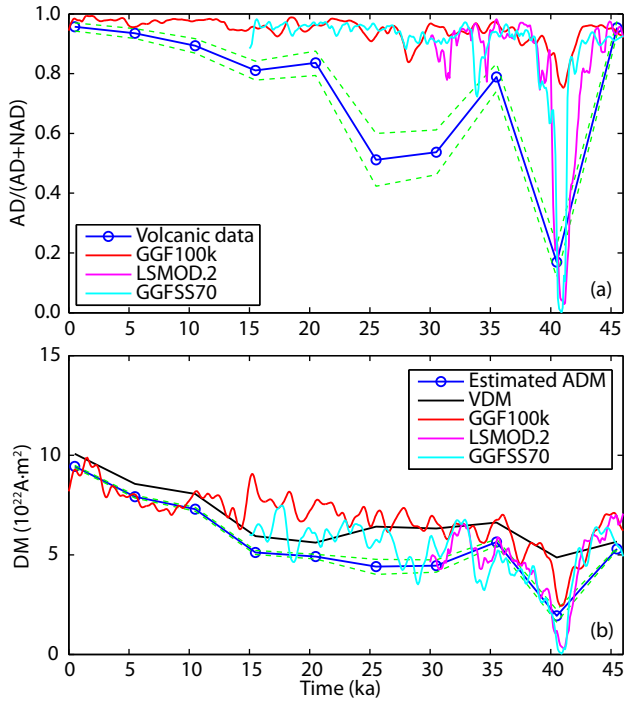

Figure 5. (a) The axial dipole/non-axial dipole (AD/NAD) ratio estimated from volcanic records (in blue) and paleomagnetic models GGF100k (in red), LSMOD.2 (in magenta), and GGFSS70 (in cyan). (b) The virtual dipole moment (VDM; in black) was derived from the volcanic records, and the axial dipole moment (ADM; in blue) was estimated from the combination of the AD/(AD + NAD) and VDM. The ADM from GGF100k, LSMOD, and GGFSS70 are denoted by the same color as that in panel (a). The green dashed lines represent the upper and lower bounds for one standard deviation in all panels. DM, dipole moment.

LSMOD.2, and GGFSS70 (Panovska et al., 2021), are plotted as red, magenta, and cyan, respectively. For the Laschamp excursion at approximately 41 ka, the results estimated by Equation (6) are close to the values obtained from the LSMOD.2 and GGFSS70 models. The AD/(AD + NAD) ratio from GGF100k was larger than that of the other three, and this finding could be attributed to the smoothness of this model. However, for the Mono Lake excursion, AD/(AD + NAD) evaluated from volcanic records using our method was lower than all the model values. During 25.5–30.5 ka, GGF100k and LSMOD.2 also showed a dip in AD/(AD + NAD), although their values significantly exceeded the estimation made directly from the volcanic inclination by using the method described above. More efforts are needed to clarify the timing and characteristics of the Mono Lake excursion. With respect to the VDM and ADM values, Figure 5b shows that from the volcanic records, all the VDM values (in black) evaluated by Equation (1) are an overvaluation of the ADM (blue), especially during the excursion times. However, the ADM estimated by using our new method exhibited good consistency with the values of the three paleomagnetic models during the Laschamp excursion time, whereas it was not significant during the Mono Lake event. This result showed that the VDM from the volcanic records was larger than the ADM values obtained from all the models for the Laschamp excursion. According to our calculations, the overestimation of the VDM by the ADM was approximately a factor of 3.

5. Discussion and Conclusions

We introduced two empirical formulae that could estimate the AD/NAD and ADM from magnetic inclination and intensity records by statistical analysis of the inclination distribution and the VDM/ADM magnitude of numerous magnetic fields from dynamo simulations. Tests of the two formulae with magnetic models demonstrated their effectiveness and helped accurately estimate the ADM during geomagnetic transition times. Applying these formulae to the volcanic records of the Laschamp excursion showed that the VDM was an overvaluation of the ADM.

These empirical formulae reflected the basic features of the inclination distribution, depending on the morphology of the geomagnetic field; thus, it is a useful tool for characterizing the morphology and ADM of the magnetic field over geological time without Gauss coefficients. Compared with the spherical harmonic method, the empirical formulae required fewer calculations. However, this empirical method requires the number of magnetic records to be at least 20 to obtain stable and reliable results. One solution is to expand the time interval to allow study of a sufficient number of records during the time period; however, this solution sacrifices temporal resolution. Considering the present collection of records, this method could play a role in investigating the magnetosphere over the past tens of thousands of years because the magnetic records were relatively rich during this period.

The RMSΔI is notably influenced by the quality and spatiotemporal distribution of the records. To better characterize the global structure of the geomagnetic field, globally widespread data distribution is necessary. Otherwise, the RMSΔI might reflect only the characteristics of the regional geomagnetic fields.

We noticed that an inversion algorithm developed recently by Rong et al. (2021) was able to quantitatively evaluate the deviations of a recorded field from a dipole field. However, their method requires that the field strength and orientation be recorded in the data set with the negligible effect of continental drift.

Because the dipole field plays an essential role in solar wind–Earth interactions, our new approach to depicting the basic morphology of the geomagnetic field will potentially benefit investigations of the space environment and biological evolution in deep geological time with the accumulation of more paleomagnetic records.

Acknowledgments, Samples, and Data

We greatly appreciate Phil Livermore and Chris J. Davies for providing the database of geodynamo simulations. This work was supported by the National Natural Science Foundation of China (Grant Nos. 41621004, 41774188). Y.W. was also supported by the Key Research Program of the Institute of Geology & Geophysics, Chinese Academy of Sciences (Grant No. IGGCAS-201904). R.N.M. was supported by the Key Research Program of the Institute of Geology & Geophysics, Chinese Academy of Sciences (Grant No. IGGCAS-201905) and the National Natural Science Foundation of China (Grant No. 41888101). GEOMAGIA50.v3 is available at

https://geomagia.gfz-potsdam.de/. The geomagnetic models mentioned in the article can be obtained from the corresponding reference papers.

References

Alken, P., Thébault, E., Beggan, C. D., Amit, H., Aubert, J., Baerenzung, J., Bondar, T. N., Brown, W. J., Califf, S., … Zhou, B. (2021). International Geomagnetic Reference Field: the thirteenth generation. *Earth, Planets Space*, *73*(1), 49. https://doi.org/10.1186/s40623-020-01288-x

Biggin, A. J., Bono, R. K., Meduri, D. G., Sprain, C. J., Davies, C. J., Holme, R., and Doubrovine, P. V. (2020). Quantitative estimates of average geomagnetic axial dipole dominance in deep geological time. *Nat. Commun.*, *11*(1), 6100. https://doi.org/10.1038/s41467-020-19794-7

Brown, M. C., Donadini, F., Korte, M., Nilsson, A., Korhonen, K., Lodge, A., Lengyel, S. N., and Constable, C. G. (2015). GEOMAGIA50.v3: 1. General structure and modifications to the archeological and volcanic database. *Earth, Planets Space*, *67*(1), 83. https://doi.org/10.1186/s40623-015-0232-0

Cassidy, J., and Hill, M. J. (2009). Absolute palaeointensity study of the Mono Lake excursion recorded by New Zealand basalts. *Phys. Earth Planet. Inter.*, *172*(3-4), 225–234. https://doi.org/10.1016/j.pepi.2008.09.018

Christensen, U. R., Aubert, J., and Hulot, G. (2010). Conditions for Earth-like geodynamo models. *Earth Planet. Sci. Lett.*, *296*(3-4), 487–496. https://doi.org/10.1016/j.epsl.2010.06.009

Davies, C. J., and Constable, C. G. (2014). Insights from geodynamo simulations into long-term geomagnetic field behaviour. *Earth Planet. Sci. Lett.*, *404*, 238–249. https://doi.org/10.1016/j.epsl.2014.07.042

Gao, J. W., Korte, M., Panovska, S., Rong, Z. J., and Wei, Y. (2022). Effects of the Laschamps excursion on geomagnetic cutoff rigidities. *Geochem., Geophys., Geosyst.*, *23*(2), e2021GC010261. https://doi.org/10.1029/2021GC010261

Glatzmaier, G. A., and Roberts, P. H. (1995). A three-dimensional self-consistent computer simulation of a geomagnetic field reversal. *Nature*, *377*(6546), 203–209. https://doi.org/10.1038/377203a0

Gong, F., Yu, Y. Q., Cao, J. B., Wei, Y., Gao, J. W., Li, H., Zhang, B. Z., and Ridley, A. (2022). Simulating the solar wind–magnetosphere interaction during the Matuyama–Brunhes paleomagnetic reversal. *Geophys. Res. Lett.*, *49*(3), e2021GL097340. https://doi.org/10.1029/2021GL097340

Grießmeier, J. M., Khodachenko, M., Lammer, H., Grenfell, J. L., Stadelmann, A., and Motschmann, U. (2009). Stellar activity and magnetic shielding. *Proc. Int. Astron. Union*, *5*(S264), 385–394. https://doi.org/10.1017/s1743921309992961

Guillou, H., Singer, B. S., Laj, C., Kissel, C., Scaillet, S., and Jicha, B. R. (2004). On the age of the Laschamp geomagnetic excursion. *Earth Planet. Sci. Lett.*, *227*(3-4), 331–343. https://doi.org/10.1016/j.epsl.2004.09.018

Korte, M., and Constable, C. G. (2005). The geomagnetic dipole moment over the last 7000 years—new results from a global model. *Earth Planet. Sci. Lett.*, *236*(1-2), 348–358. https://doi.org/10.1016/j.epsl.2004.12.031

Korte, M., Brown, M. C., Panovska, S., and Wardinski, I. (2019). Robust characteristics of the Laschamp and Mono Lake geomagnetic excursions: results from global field models. *Front. Earth Sci.*, *7*, 86. https://doi.org/10.3389/feart.2019.00086

Leonhardt, R., and Fabian, K. (2007). Paleomagnetic reconstruction of the global geomagnetic field evolution during the Matuyama/Brunhes transition: iterative Bayesian inversion and independent verification. *Earth Planet. Sci. Lett.*, *253*(1-2), 172–195. https://doi.org/10.1016/j.epsl.2006.10.025

Leonhardt, R., Fabian, K., Winklhofer, M., Ferk, A., Laj, C., and Kissel, C. (2009). Geomagnetic field evolution during the Laschamp excursion. *Earth Planet. Sci. Lett.*, *278*(1-2), 87–95. https://doi.org/10.1016/j.epsl.2008.11.028

Meduri, D. G., Biggin, A. J., Davies, C. J., Bono, R. K., Sprain, C. J., and Wicht, J. (2021). Numerical dynamo simulations reproduce paleomagnetic field behavior. *Geophys. Res. Lett.*, *48*(5), e2020GL090544. https://doi.org/10.1029/2020GL090544

Merrill, R. T., McElhinny, M. W., and McFadden, P. L. (1998). *The Magnetic Field of the Earth: Paleomagnetism, the Core, and the Deep Mantle*. San Diego, California: Academic Press.

Panovska, S., Constable, C. G., and Korte, M. (2018). Extending global continuous geomagnetic field reconstructions on timescales beyond human civilization. *Geochem., Geophys., Geosyst.*, *19*(12), 4757–4772. https://doi.org/10.1029/2018GC007966

Panovska, S., Korte, M., and Constable, C. G. (2019). One hundred thousand years of geomagnetic field evolution. *Rev. Geophys.*, *57*(4), 1289–1337. https://doi.org/10.1029/2019RG000656

Panovska, S., Korte, M., Liu, J. B., and Nowaczyk, N. (2021). Global evolution and dynamics of the geomagnetic field in the 15–70 kyr period based on selected paleomagnetic sediment records. *J. Geophys. Res.: Solid Earth*, *126*(12), e2021JB022681. https://doi.org/10.1029/2021JB022681

Rong, Z. J., Wei, Y., Klinger, L., Yamauchi, M., Xu, W. Y., Kong, D. L., Cui, J., Shen, C., Yang, Y. Y., … Chai, L. H. (2021). A new technique to diagnose the geomagnetic field based on a single circular current loop model. *J. Geophys. Res.: Solid Earth*, *126*(11), e2021JB022778. https://doi.org/10.1029/2021JB022778

Smith, P. J. (1967). The intensity of the ancient geomagnetic field: a review and analysis. *Geophys. J. R. Astron. Soc.*, *12*(4), 321–362. https://doi.org/10.1111/j.1365-246X.1967.tb03146.x

Sprain, C. J., Biggin, A. J., Davies, C. J., Bono, R. K., and Meduri, D. G. (2019). An assessment of long duration geodynamo simulations using new paleomagnetic modeling criteria (Q_{PM}). *Earth Planet. Sci. Lett.*, *526*, 115758. https://doi.org/10.1016/j.epsl.2019.115758

Stadelmann, A., Vogt, J., Glassmeier, K. H., Kallenrode, M. B., and Voigt, G. H. (2010). Cosmic ray and solar energetic particle flux in paleomagnetospheres. *Earth, Planets Space*, *62*(3), 333–345. https://doi.org/10.5047/eps.2009.10.002

Tauxe, L., and Kent, D. V. (2004). A simplified statistical model for the geomagnetic field and the detection of shallow bias in paleomagnetic inclinations: was the ancient magnetic field dipolar?. In J. E. T. Channell, et al. (Eds.), *Timescales of the Paleomagnetic Field* (Vol. 145, pp. 101–115). Washington, DC: American Geophysical Union.

Tsareva, O. O., Dubinin, E. M., Malova, H. V., Popov, V. Y., and Zelenyi, L. M. (2020). Atmospheric escape from the Earth during geomagnetic reversal. *Ann. Geophys.*, *63*(2), PA223. https://doi.org/10.4401/ag-8354

Vogt, J., Zieger, B., Glassmeier, K. H., Stadelmann, A., Kallenrode, M. B., Sinnhuber, M., and Winkler, H. (2007). Energetic particles in the paleomagnetosphere: reduced dipole configurations and quadrupolar contributions. *J. Geophys. Res.*, *112*(A6), A06216. https://doi.org/10.1029/2006ja012224

Wei, Y., Pu, Z. Y., Zong, Q. G., Wan, W. X., Ren, Z. P., Fraenz, M., Dubinin, E., Tian, F., Shi, Q. Q., … Hong, M. H. (2014). Oxygen escape from the Earth during geomagnetic reversals: implications to mass extinction. *Earth Planet. Sci. Lett.*, *394*, 94–98. https://doi.org/10.1016/j.epsl.2014.03.018